AIChE WILEY InterScience DISCOVER SOMETHING GREAT

Validation of Bivariate DQMOM for Nanoparticle Processes Simulation

Alessandro Zucca, Daniele L. Marchisio, Marco Vanni, and Antonello A. Barresi
Dip. Scienza dei Materiali e Ingegneria Chimica - Politecnico di Torino,
C.so Duca degli Abruzzi 24 - 10129 - Torino - Italy

DOI 10.1002/aic.11125
Published online February 16, 2007 in Wiley InterScience (www.interscience.wiley.com).

Since it was first proposed, the direct quadrature method of moments (DQMOM) has been employed for the solution of population balance equations in a wide range of applications. One of its most interesting features is that it can be easily employed for the solution of multivariate population balances, which are often necessary to obtain complete information on the particle population under study. In addition, DQMOM can be easily implemented in computational fluid dynamic (CFD) codes, and requires low computational costs. A bivariate formulation of the population balance equation that is particularly suited for modeling nanoparticles formation in flames is presented. The use of DQMOM for the solution of bivariate population balances is explored in detail, and the method is validated by comparison with simulations carried out with a code based on Monte Carlo methods (MCM). Particular attention is devoted to the choice of the moments to be tracked in DQMOM, in order to obtain a stable algorithm and reliable and accurate results. Eventually the method is implemented in a commercial CFD code, and a real application is studied: soot nanoparticles formation in turbulent combustion processes. © 2007 American Institute of Chemical Engineers *AIChE J,* 53: 918–931, 2007
Keywords: population balance equation, moments method, Monte Carlo, aggregation, sintering

Introduction

Detailed mathematical modeling of particulate systems has recently attracted the growing interest of the scientific and engineering communities for its several applications, for example, simulation of soot nanoparticles formation in combustion processes, assessment of their evolution in the environment, and their effects on climate change and optimization of flame aerosol synthesis for industrial production of catalyst and ceramic nanoparticles.

Combustion processes in general and diesel engines in particular are the major sources in developed countries of black carbon aerosol, also known as soot, which is formed by incomplete oxidation of the species that constitute the fuel, with the production of benzene molecules, which grow to give polycyclic aromatic hydrocarbons, considered key compounds in the reactions involved in the first stages of the process.[1] Researchers are particularly worried about the threat that it represents for human health and about the effect that soot has on the ability of the snow to reflect the sunlight, resulting in climate changes from the Arctic to the Alps. Mathematical models able to describe the formation of soot in combustion processes are profitably used for design, optimization and scale-up of industrial low-emission combustors.[2] Moreover, since mixing plays a fundamental role also in soot transport in the environment, the same mathematical framework can be used to describe and predict its geographical distribution, and, therefore, to characterize its influence on climate.[3,4]

The very same principles can be applied for modeling flame aerosol synthesis. This process is used to produce on the industrial scale nanoparticles with controlled characteristics for several applications, such as materials for catalysis, pigments and additives. The process consists of spraying a

Correspondence concerning this article should be addressed to D. L. Marchisio at daniele.marchisio@polito.it.

solution containing the precursor in a high-temperature flame. Due to the high-temperature the solvent evaporates, and the precursor precipitates forming nanosized nuclei that quickly aggregate through Brownian aggregation. Temperature profiles and flame characteristics determine the condition of formation (nucleation), and of evolution (molecular growth and aggregation) of these particles, and the flame can be controlled in order to produce particles with desired characteristics. Again, a mathematical model can be used to describe the phenomena involved,[5] to better understand the experimental results obtained,[6,7] and to develop a consistent theory for design and optimization.

A proper and accurate simulation of these processes must take into account the evolution of the particulate phase, its interactions with the surrounding fluid phase and the effect of mixing. Very often these elements are deeply linked together so that all these phenomena must be described within the same mathematical framework. This issue can be successfully addressed by using computational fluid dynamics (CFD), which was shown to be a very useful and accurate modeling framework for the description of particulate systems, and for the description of turbulent flows in general.[8,9]

In order to describe the evolution of the disperse particulate phase, CFD must be coupled with a population balance equation (PBE). The population balance model must be easily implementable in a CFD code, computationally affordable and must describe accurately the particulate phase. Many numerical approaches can be used to solve this equation, such as classes methods (CM), Monte Carlo methods (MCM), and method of moments (MOM), and for details one can see the book by Ramkrishna.[10] Classes methods are the most popular,[11–13] whereas MCM are well known for their ease of implementation. Both methods theoretically present no limitation in the number of properties of the population that can be tracked, however, in both cases dimensionality reduces accuracy. In Monte Carlo approaches this is caused by the insufficient sampling from the full set (that is, limited number of notional particles), while in classes methods this limitation is caused by the poor accuracy associated to the limited number of classes.

The MOM was formulated in the 60s,[14] and since then mainly abandoned for the so-called closure problem. Recently, the closure problem has been reviewed[15] and a new method known as quadrature method of moments (QMOM) has been proposed,[16] validated[17–19] and applied for studying a wide range of practical problems.[20–25] The main limitation of the classical QMOM is that it can treat only PBE tracking one property of the population of particles, such as particle mass, size, volume or area (that is, monovariate PBE). However, as it will become clearer later, in a number of practical cases it is interesting to describe the population of particles with bivariate (or multivariate) PBE, where two or more properties of the population are simultaneously tracked (for example, particle volume and particle area). This is particularly interesting in the case of aggregation and breakage of fractal clusters, and for this reason QMOM has been extended to bivariate problems.[26–28] QMOM has been also formulated in different direct ways[4,29] and the so-called direct quadrature method of moments (DQMOM)[30,31] seems to be a very interesting method for bi- and multivariate PBE.

In this work we focus on the use of DQMOM for solving bivariate PBEs, and we assess the accuracy of the method by comparison with simulations carried out with MCM that, as already stated, is an accurate computational tool for studying multivariate populations. It is important to highlight that this approach in a truly bivariate formulation has never been validated. In fact previous applications and validations were carried out in pseudo bivariate cases, where the bivariate problem was handled using algebraic relationships between the involved internal coordinates, as for example in the case of particle size and velocity,[30] resulting in actual monovariate problems. Moreover, in its original formulation[31] some important technical and numerical issues were only tagged, but not completely understood and properly addressed.

In order to effectively address all these issues the validation in this work is carried out with a limited number of test cases that are relevant for a specific application: the simulation of nanoparticle formation and evolution. Our results show that DQMOM is a stable and accurate method for describing the evolution of a population of nanoparticles undergoing molecular growth, Brownian aggregation, breakage, and sintering/restructuring, and presents the great advantage of being computationally affordable, and, therefore, can be easily implemented in CFD codes. Eventually the method is implemented in a commercial CFD code (Fluent 6.2), and a real process is described: soot nanoparticles formation in turbulent combustion.

Monovariate vs. bivariate particle description

In typical applications, the population of particles under study can undergo several phenomena, such as nucleation, molecular growth, sintering, restructuring, aggregation and breakage. Nucleation is the formation of a small particle of the solid phase within the continuous-fluid phase and produces a *nucleus* of specific size. Because of molecular growth and aggregation nuclei can grow forming complex clusters. These clusters or aggregates can be very sparse with open and loose structures or more compact, almost as solid spheres. The structure of aggregates is directly linked to the controlling mechanism. In fact, very fast aggregation rates usually cause the formation of sparse and loose aggregates, whereas slow aggregation rates result in more compact aggregates. Also subsequent mechanisms strongly influence the aggregate structure, for example restructuring due to external forces (for example, shear stresses) can make the cluster more compact. Other continuous processes, such as molecular growth, can have a strong effect too; in fact, if molecular growth fills the empty spaces between primary particles the resulting structure of the aggregate is strongly changed; this is usually referred to as condensational obliteration.[32]

When all the particles have a well-defined shape which is not changed during the evolution of the population, as in the case of coalescence of drops or bubbles, or when the information on particle morphology is not needed, the solution of the monovariate population balance is suitable to describe the system, which is fully characterized by one internal coordinate (for example, volume or mass, characteristic diameter, number of primary particles per aggregate).

On the contrary, when particle structure evolves in time, as in the case of solid particle aggregation, breakage and

restructuring, knowledge of particle mass or volume is not sufficient to infer any further information on particle morphology; in this case, a bivariate PBE must be solved, as at least two particle properties need to be tracked independently. The second internal coordinate can be the fractal dimension,[33–35] or another property of the population, for example, the actual surface area, or the radius of gyration. It is important to highlight that this modeling choice is strongly problem-dependent, and for different problems different additional properties should be used. Yet the DQMOM approach is fully general, and is valid for any selection of coordinates. As suggested by several authors the second independent property could be the actual external surface area of the particle, A. In this case, when two particles collide the resulting surface is the summation of the surface areas of the two original particles and, subsequently, because of sintering or restructuring, the surface area of the particles can be reduced.[26]

Number-density function and population-balance equation

If particle volume V and particle area A are used as independent population properties, we can introduce the *number-density function* $n(V,A;\mathbf{x},t)$ so that $n(V,A;\mathbf{x},t)dVdAd\mathbf{x}$ is the number of particles contained in an infinitesimal volume $d\mathbf{x}$ around the physical point $\mathbf{x}$, at the instant t, with volume and area in the range $[V,\ V+dV]$ and $[A,\ A+dA]$. Volume and area are labelled as *internal coordinates* to distinguish them from the spatial coordinates, known as external coordinates. It follows that the total number density (that is, total number of particles per unit volume) is

$$N(\mathbf{x},t)=\int_0^{+\infty}\int_0^{+\infty} n(V,A;\mathbf{x},t)dVdA. \tag{1}$$

For the study of particle dynamics considered in this work, the PBE is as follows (repeated indices imply summation)

$$\frac{\partial n(V,A)}{\partial t}+\frac{\partial}{\partial x_i}\left[u_i\, n(V,A)\right]-\frac{\partial}{\partial x_i}\left[\Gamma\frac{\partial n(V,A)}{\partial x_i}\right] =-\frac{\partial}{\partial V}\left[\dot{V}\, n(\dot{V},A)\right]-\frac{\partial}{\partial A}\left[\dot{A}\, n(V,A)\right]+h(V,A), \tag{2}$$

where the first term on the lefthand side of Eq. 2 is the accumulation term, whereas the second one is convection in physical space, namely the transport of particles due to their velocity u_i. The third term on the lefthand side is the diffusion term, which represents transport due to diffusion processes, such as Brownian motion or turbulent fluctuations, and Γ is the resulting diffusion coefficient. The terms on the lefthand side account for time and spatial transport and when Eq. 2 is solved with a commercial CFD code, these terms are usually taken care of by the code itself. All the other terms, that do not represent time and spatial transport, are grouped together into one single term (that is, $S(V,A)$). The first and second terms on the righthand side are due to continuous changes of particle volume and particle area; $\dot{V}$ individuates the rate of change of particle volume due to continuous processes, whereas $\dot{A}$ is the rate of change of particle area due to continuous phenomena (for example, restructuring and sintering). In the case of restructuring and sintering, this term is usually written as[35,36]

$$\dot{A}=-\gamma(A-A_{\min}) \tag{3}$$

where γ is the restructuring (or sintering) rate, whereas the driving force is the difference between the area of the aggregate and the minimum area. This latter quantity is the minimum area physically allowed for the same aggregate in the considered operating conditions.

The third term on the righthand side of Eq. 2 is due to discrete events, such as nucleation, aggregation and breakage. Let us analyze in detail aggregation and breakage, since nucleation has been analyzed elsewhere.[31] In the case of pure aggregation the source term is as follows

$$h(V,A)=\frac{1}{2}\int_0^A\int_0^V a(\tilde{V},V',\tilde{A},A')n(\tilde{V},\tilde{A}) \times n(V',A')\left|\frac{\partial(\tilde{V},\tilde{A})}{\partial(V',A')}\right|dV'dA'-n(V,A) \times\int_0^{+\infty}\int_0^{+\infty} dV_{\xi'}a(V,V',A,A')n(V',A')dV'dA' \tag{4}$$

where the aggregation kernel $a(\tilde{V},V',\tilde{\mathrm{A}},A')$ measures the frequency of successful collisions and consequent aggregation of particles whereas the determinant of the Jacobian $|\frac{\partial(\tilde{V},\tilde{A})}{\partial(V',A')}|$ is needed for the variable transformation in the integral.[10]

In the case of aggregation of rigid particles, with particle volume and particle surface area as internal coordinates, volume V is additive, as well as the actual surface area A:

$$V=\tilde{V}+V', \tag{5}$$

$$A=\tilde{A}+A', \tag{6}$$

and it is easy to show that in this case the determinant of the Jacobian is equal to one. The fact that during aggregation both volume and area are additive implies that the area is the real surface area (including the surface area of internal porosity) of an aggregate composed by a number of primary particles connected by ideal contact points. If $\dot{V}$ or $\dot{A}$ are null the bivariate description is redundant. If $\dot{V}$ or $\dot{A}$ are instead non-null, the final particle volumes and surface areas will result from the competition of aggregation, sintering (or restructuring) and molecular growth, and the bivariate description is needed.[26]

Let us consider now the source term due to pure breakage

$$h(V,A)=\int_A^{+\infty}\int_V^{+\infty} b(V',A')P(V,A|V',A')n(V',A')dV'dA' -b(V,A)n(V,A), \tag{7}$$

where the breakage kernel $b(V',A')$ is the frequency of fragmentation of a particle with (V',A'), whereas $P(V,A|V',A')$ is the *daughter-distribution function*, namely the volume and area distribution of daughter particles (V,A) formed by fragmentation of a mother particle (V',A'). Typical kernels valid for breakage of solid particles are the exponential kernel,[37] and the power-law kernel;[38] typical daughter-distribution functions are those characterizing symmetric breakage (that is, rup-

ture with formation of equal particles), and erosion (that is, removal of a primary particle from a big aggregate). In the case of symmetric breakage, the daughter-distribution function is

$$P(V,A|V',A') = 2\delta\left(V - V'/2\right)\delta\left(A - A'/2\right), \qquad (8)$$

assuming, for example, that both the volume and the area of the daughter particles are half of the mother particle.

Solution of the population-balance equation

As already reported, the population balance equation can be solved with different numerical approaches, which present advantages and drawbacks. Let us consider with major detail the direct quadrature method of moments (DQMOM), and the Monte Carlo method (MCM) used in this work.

Direct Quadrature Method of Moments. This approach is based on the solution of the population balance in terms of the moments of the number-density function. For the bivariate number density function introduced earlier the mixed moment of order k and l with respect to volume and area is as follows

$$m_{kl}(\mathbf{x},t) = \int_0^{+\infty}\int_0^{+\infty} n(V,A;\mathbf{x},t)V^k A^l dV dA \qquad (9)$$

and it is clear that m_{00} is the total particle number density (see Eq. 1), m_{10} is the total particle volume, and m_{01} is the total particle area. From these mixed moments the average particle volume can be obtained as the ratio of m_{10} and m_{00}, whereas the average particle area is the ratio of m_{01} and m_{00}. Also other mixed moments have particular physical meaning and can be related to measurable quantities.[39]

McGraw showed that a convenient approach for overcoming the closure problem is the use of a quadrature approximation of order N that corresponds to the approximation of the number-density function as the summation of N delta functions[16,31]

$$n(V,A;\mathbf{x},t) = \sum_{\alpha=1}^{N} w_\alpha(\mathbf{x},t)\delta[V - V_\alpha(\mathbf{x},t)]\delta[A - A_\alpha(\mathbf{x},t)], \qquad (10)$$

where $w_a(\mathbf{x},t)$ are the *weights*, and where $V_a(\mathbf{x},t)$ and $A_a(\mathbf{x},t)$ are the *abscissas* or *nodes* of the quadrature approximation, that can be calculated from the mixed moments of the distribution

$$m_{kl}(\mathbf{x},t) = \int_0^{+\infty}\int_0^{+\infty} n(V,A;\mathbf{x},t)V^k A^l dV dA \approx \sum_{\alpha=1}^{N} w_\alpha V_\alpha^k V_\alpha^l \qquad (11)$$

using the product-difference (PD) algorithm[40] for monovariate PBE or resorting to its extension for bivariate PBE.[26–28,41] When DQMOM is used the transport equations for weights and abscissas are directly solved, forcing the quadrature approximation to yield correct values of the selected set of moments.[31] One of the main advantages of this technique is that accounting for more than one internal coordinate does not increase significantly the complexity of the algorithm, that represents an important issue that did not find a convenient solution in alternative approaches. For example, in the bivariate case, the method requires the solution of transport equations for $3N$ scalars (that is, N weights and $2N$ abscissas)

$$\frac{\partial w_\alpha}{\partial t} + \frac{\partial}{\partial x_i}\left[u_i\, w_\alpha\right] - \frac{\partial}{\partial x_i}\left[\Gamma\frac{\partial w_\alpha}{\partial x_i}\right] = a_\alpha$$

$$\frac{\partial (w_\alpha V_\alpha)}{\partial t} + \frac{\partial}{\partial x_i}\left[u_i (w_\alpha V_\alpha)\right] - \frac{\partial}{\partial x_i}\left[\Gamma\frac{\partial (w_\alpha V_\alpha)}{\partial x_i}\right] = b_{V\alpha}$$

$$\frac{\partial (w_\alpha A_\alpha)}{\partial t} + \frac{\partial}{\partial x_i}\left[u_i\, (w_\alpha A_\alpha)\right] - \frac{\partial}{\partial x_i}\left[\Gamma\frac{\partial (w_\alpha A_\alpha)}{\partial x_i}\right] = b_{A\alpha} \qquad (12)$$

where a_α $b_{V\alpha}$ and $b_{A\alpha}$ are the $3N$ relative source terms ($\alpha = 1,\ldots,N$). A graphical representation of the bivariate quadrature approximation on which the DQMOM is based is depicted in Figure 1, where a bivariate number-density function and its DQMOM representation are compared.

The $3N$ source terms can be easily evaluated by solving a linear algebraic system, obtained from the population balance equation after the application of the quadrature approximation and forcing the moments to be tracked with high accuracy. In fact, if we substitute Eq. 10 into Eq. 2, and rewrite the population balance in terms of the moments of the distribution, we obtain the following equation

$$\sum_{\alpha=1}^{N}\left[(1-k-l)V_\alpha^k A_\alpha^l a_\alpha + kV_\alpha^{k-1}A_\alpha^l b_{V\alpha} + lV_\alpha^k A_\alpha^{l-1} b_{A\alpha}\right] = \bar{C}_{kl} + \bar{S}_{kl}^{(N)}. \qquad (13)$$

If Eq. 13 is applied for $3N$ different moments a linear system is obtained, where $\bar{S}_{kl}^{(N)}(\mathbf{x}, t)$ is the quadrature approximation with N nodes of the moment transform of the source term of order k with respect to the first internal coordinate (V), and

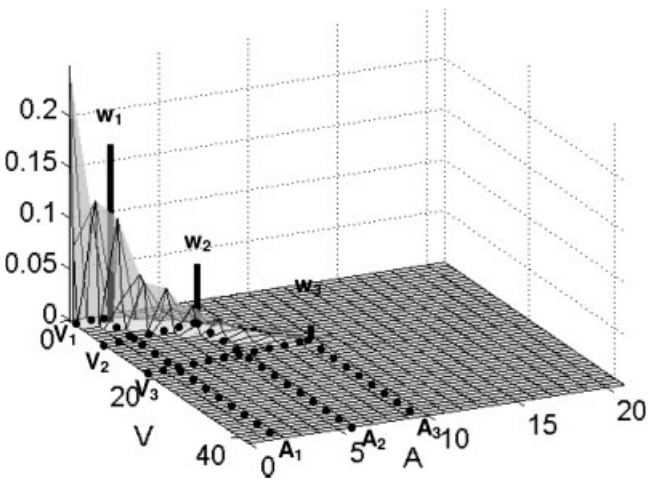

Figure 1. Comparison between a bivariate number density function with respect to surface area and volume, and its quadrature approximation with three nodes (black peaks).

of order l with respect to the second internal coordinate (A)

$$\bar{S}_{kl}^{(N)}(\mathbf{x},t) \approx \bar{S}_{kl}(\mathbf{x},t) = \int_0^{+\infty}\int_0^{+\infty} S(V,A)V^k A^l dVdA, \quad (14)$$

and its functional form is reported for several cases in Eqs. 17–22, whereas $\overline{C}_{kl}$ is a correction term which is needed due to the finite-mode representation of the distribution, and is effective only for moments of order two or higher. It is a function of the gradients of the nodes, and is evaluated as follows

$$\bar{C}_{kl} = \Gamma \sum_{\alpha=1}^{N} w_\alpha \left[k(k-1)V_\alpha^{k-2}A_\alpha^l \frac{\partial V_\alpha}{\partial x_i}\frac{\partial V_\alpha}{\partial x_i} + 2klV_\alpha^{k-1}A_\alpha^{l-1}\frac{\partial V_\alpha}{\partial x_i}\frac{\partial A_\alpha}{\partial x_i} + l(l-1)V_\alpha^k A_\alpha^{l-2}\frac{\partial A_\alpha}{\partial x_i}\frac{\partial A_\alpha}{\partial x_i}\right] \quad (15)$$

If two nodes are employed (that is, $N = 2$), then two weights w_1 and w_2 and four abscissas (V_1, V_2, A_1 and A_2) are tracked, and, therefore, in order to solve their six transport equations, six unknown source terms (a_1, a_2, b_{V1}, b_{V2}, b_{A1}, b_{A2}) must be calculated. This can be done by solving the linear system of Eq. 13 generated by six different combinations of moment orders k and l, or in other words by forcing the quadrature approximation to correctly evaluate for that specific instant the source terms of the six moments of the distribution.

Of course, if three nodes (that is, $N = 3$) are considered, the values of three weights w_1, w_2 and w_3, and of six abscissas V_1, V_2, V_3 and A_1, A_2, A_3, for a total of nine unknown source terms (a_1, a_2, a_3, b_{V1}, b_{V2}, b_{V3}, b_{A1}, b_{A2},b_{A3}) must be determined. As a consequence, one needs to select nine mixed moments of the distribution.

The linear system can be solved only if it is nonsingular, and only if the vector on the righthand side is known. As already reported the latter is constituted by the source terms of the moments and the correction terms. The moment source terms contain different contributions from the processes involved (that is, nucleation, growth, sintering, aggregation and breakage).

In the case of aggregation of solid particles (that is, additive volume and surface area, and ideal contact points) the source term due to aggregation becomes

$$\bar{S}_{kl} = \frac{1}{2}\iiiint_0^{\infty}\left[(V+V')^k(A+A')^l - V^kA^l - V'^kA'^l\right] a(V,V',A,A')n(V,A)n(V',A')dVdV'dAdA', \quad (16)$$

and after applying the quadrature approximation

$$\bar{S}_{kl}^{(N)} = \frac{1}{2}\sum_{\alpha=1}^{N}\sum_{\beta=1}^{N}\left[(V_\alpha+V_\beta)^k(A_\alpha+A_\beta)^l - V_\alpha^kA_\beta^l - V_\alpha^kA_\beta^l\right]a_{\alpha\beta}w_\alpha w_\beta. \quad (17)$$

In the case of pure breakage

$$\bar{S}_{kl} = \int V^k \int A^l \int\int_0^{\infty} b(V',A')P(V,A|V',A') \times n(V',A')dV'dA'dVdA - \int V^k \int_0^{\infty} A^l b(V,A)n(V,A)dVdA \quad (18)$$

and, after the application of the quadrature approximation

$$\bar{S}_{kl}^{(N)} = \sum_{\alpha=1}^{N}(\bar{P}_\alpha^{kl} - 1)b_\alpha V_\alpha^k A_\alpha^l w_\alpha, \quad (19)$$

where $b_\alpha = b(V_\alpha, A_\alpha)$, and where for the case of symmetric breakage

$$\bar{P}_\alpha^{kl} = \int\int_0^{\infty} P(V,A|V_\alpha,A_\alpha)V^kA^l dVdA = 2^{1-k-l}V_\alpha^kA_\alpha^l. \quad (20)$$

When considering continuous changes with a bivariate PBE, we can account for the drift term for each coordinate independently. If we denote with $\dot{V}(V,A)$ and $\dot{A}(V,A)$ the rates of continuous change of volume and surface area, respectively, the source term of the moments is

$$\bar{S}_{kl} = \int_0^{\infty}\frac{\partial}{\partial A}\left[\dot{A}(V,A)n(V,A)\right]V^kA^l dVdA + \int_0^{\infty}\frac{\partial}{\partial V}\left[\dot{V}(V,A)n(V,A)\right]V^kA^l dVdA, \quad (21)$$

and applying the quadrature approximation, results in

$$\bar{S}_{kl}^{(N)} = \sum_{\alpha=1}^{N} w_\alpha\left[kV_\alpha^{k-1}A_\alpha^l\dot{V}_\alpha + lV_\alpha^kA_\alpha^{l-1}\dot{A}_\alpha\right] \quad (22)$$

where, as before $\dot{V}_\alpha = \dot{V}(V_\alpha, A_\alpha)$ and $\dot{A}_\alpha = \dot{A}(V_\alpha, A_\alpha)$.

The choice of the set of moments that generate the linear system is nontrivial and affects both the accuracy and the stability of the method. First, the tracked moments are predicted with high-accuracy, while one cannot be sure of the accuracy of the other moments extrapolated from the quadrature approximation. However, this issue is problem-dependent, and, therefore, will be discussed in details for the practical cases tested in this work.

Second, the chosen set of moments affects the numerical stability of the method, resulting in either well-conditioned or ill-conditioned problems. The problem becomes ill-conditioned when the linear system becomes nearly singular, and generally this happens if two nodes of the quadrature approximation approach each other at least for one of the internal coordinates. In this case, the accuracy in the computation of source terms for weights and abscissas can be dramatically reduced, thus, leading to inaccuracy and to numerical instability. The more the linear system is kept far from singularity during the computation, the more accurate is the prediction of both tracked and nontracked moments, and the easier and faster is the computation. Of course, as the number of nodes increases, the probability of finding two nodes approaching each other is higher. Therefore, the first conclusion that can be drawn is that a large number of nodes should be avoided if possible. Another factor affecting numerical stability is the order of the mixed moments used to compute the source terms for weights and abscissas. In general, the higher is the order of the chosen moments, the stiffer is the solution of the linear system. From this point of view one should avoid to include higher-order moments that do not need to be known with high-accuracy. With this respect, it is indeed interesting the possibility of using fractional moments. Also this issue is

problem-dependent, and must be discussed for each practical case separately.

The last requirement that must be fulfilled is that the set of moments leads to a nonsingular linear system. Differently from previous cases this last issue depends only on the choice of the moments, notwithstanding the particular problem under study. This is due to the fact that since DQMOM uses a limited number of nodes, it is impossible to express all the mixed moments independently. Due to the finite-mode representation, in fact, some mixed moments are actually linear combination of other moments, and, therefore, when chosen for the construction of the linear system lead to a singular one.

For example, let us consider a bivariate distribution described with a quadrature approximation with two nodes (that is, six variables: two weights and two abscissas for each internal coordinate). In order to solve Eq. 13 one needs to choose six moments. In general the first three moments (m_{00}, m_{10}, m_{01}) will always be selected since they represent important properties of the population (that is, total particle-number density and total volume and area), and three more moments must be selected. For example, a singular system is obtained when the first six integer mixed moments (that is, m_{00}, m_{10}, m_{01}, m_{20}, m_{11}, m_{02}) are chosen. In this case singularity is caused by the linear dependency of the moments, in fact using two nodes, m_{11} (that is, covariance) is a linear combination of m_{02} and m_{20} (that is, pure variances), meaning that two points in the particle volume/particle area-phase plane will always be aligned! Similarly, it is possible to show that choosing any tern of pure moments of a single internal coordinate (for example, m_{20}, m_{30}, m_{40}) a singular linear system is obtained. However, any other combination of pure moments of both the internal coordinates leads to nonsingular systems.

If three nodes are employed, and if the analysis is restricted to the sets including the first five pure moments (that is, m_{00}, m_{10}, m_{01}, m_{20}, m_{02}), it appears that it is sufficient not to include m_{11} to avoid singularity. In fact, in this case it is possible to have the covariance (that is, m_{11}) linearly independent from the pure variances (that is, m_{02} and m_{20}), because in the particle volume/particle area phase plane three points can also be not aligned. It is interesting to notice that all the sets containing five of the first six moments lead to a nonsingular system.

Monte Carlo Method. In MCM the evolution of the particulate system is simulated by considering a statistically significant number of notional particles undergoing a large number of randomly selected events, each of them artificially realizing a physical event involving real particles. Monte Carlo simulations describe realistically and accurately the behavior of the physical system, provided that the number of particles considered is large enough to have statistical reliability; moreover, they can provide very detailed information on the population. Monte Carlo simulations are not usually coupled with CFD computations, due to their large computational cost, but can be successfully employed to validate simplified models. In the following we briefly describe the in-house Monte Carlo code employed in this work for the validation of bivariate DQMOM.

The simulation framework operates on a closed system of volume V, subdivided in N_s smaller well mixed volumes V_v, called "reservoirs", each of them able to exchange particles with the other ones. As suggested by Liffmann,[42] the code considers only a subvolume of each reservoir $\Delta V_v = \alpha V_v$, with $\alpha \ll 1$ in order to deal with a reasonable number of particles. The possible processes are aggregation between two particles belonging to the same subvolume, breakage of a particle, and escape of a particle from a subvolume toward a different reservoir, because of convection and diffusion. The frequency of each event can be computed from the aggregation and breakage kernels, and from the average-residence time in reservoir v for the escape process. If we define the total event frequency f_{tot} as the sum of the frequencies of all possible events, we can determine the time interval between two events (Δt) by sampling from a random variable with cumulative probability distribution given by

$$\Pr(\Delta t) = 1 - e^{f_{tot}\Delta t}. \tag{23}$$

When the time at which the new event occurs has been determined, we have to choose the event among all the possible ones. The selection of the event is governed by the inversion method:[43–45] the possible events are ordered, a random number ξ is picked from a uniform distribution between 0 and 1, and the event q, that satisfies the following relationship is selected

$$\sum_{k=1}^{q-1} \Pr_k < \xi \leq \sum_{k=1}^{q} \Pr_k, \tag{24}$$

where $\Pr_k = f_k/f_{tot}$ is the probability of the generic event k. A similar procedure is used, when a particle escapes, to select the destination reservoir.

If the aggregation rate is much larger than breakage rate, after some time the number of particles can be too small to guarantee statistical reliability; when breakage is the dominant process, on the other side, the number of particles can become so large that the computation time can be no more acceptable. To avoid these problems the total number of particles must remain nearly constant; this is obtained by doubling the volume and the population if

$$N_p < N_{p,\min} = \frac{3}{4}N_{p,0} - 2N_v, \tag{25}$$

and halving the volume and the population (by random decimation) if

$$N_p > N_{p,\max} = \frac{3}{2}N_{p,0} + 2N_v. \tag{26}$$

In Eqs. 25 and 26, N_p is the total number of particles, $N_{p,0}$ is the initial number of particles, and the terms $\pm 2N_v$ are introduced to avoid rapid halving-doubling sequences during the simulation.

Test cases and numerical details

The performance of DQMOM has been investigated in different test cases and results have been validated by comparison with Monte Carlo simulations. For all the test cases, DQMOM was implemented in MatLab® 6.5, whereas the Monte Carlo method was implemented with an in-house code in Fortran. Both DQMOM and Monte Carlo simulations were run on an Intel® Xeon™ CPU 2.80 GHz, 1.00 GB

RAM. The typical CPU time for a DQMOM simulation was of the order of seconds up to some minutes, whereas for a Monte Carlo simulation ranged from few hours to some days, depending on the complexity of the simulation.

As it has been stated before, Monte Carlo predictions are used here as a reference, and usually their accuracy for low-order moments is very high when working with a reasonable number of particles (that is, $10^3 - 10^4$). More problematic is the calculation of higher-order moments: in fact, if the number of particles employed is not large enough to capture the tails of the distribution higher-order moments can be seriously underestimated. In order to verify the accuracy of the MCM, results obtained with different numbers of particles were compared. The analysis showed that for moments of order smaller than four, no significant difference was detected when increasing the number of particles from 10^4 to 10^5, whereas for fourth-order moments the discrepancy was smaller than 5%, and smaller than 10% for most of the fifth-order moments. These results lead to the conclusion that the improvement that could be obtained using a larger number of particles for the Monte Carlo simulation (with a very large increase in the computation time) would not significantly modify the conclusions that can be drawn comparing DQMOM with the Monte Carlo simulation with 10^5 particles.

The first case investigated is aggregation, breakage and sintering/restructuring of rigid particles in a homogeneous system without spatial gradients. Simulations were carried out considering Brownian aggregation with the following kernel

$$a_{\alpha\beta} = a_0 \frac{\left(V_\alpha^{1/3} + V_\beta^{1/3}\right)^2}{V_\alpha^{1/3} V_\beta^{1/3}} \tag{27}$$

where $a_0 = 10^{-2}$ m^3/s, and a constant kernel with $a_{\alpha\beta} = a_0 = 4 \times 10^{-2}$ m^3/s. Brownian and constant kernels were chosen here as test cases, because these are the most widely used is the description of nanoparticle aggregation, since in this case Brownian motion is the dominant aggregation mechanism. The sintering/restructuring rate is expressed in terms of the law reported in Eq. 3 that after the application of the quadrature approximation becomes

$$\dot{A}_\alpha = -\gamma(A_\alpha - A_{\alpha,\min}), \tag{28}$$

where $\gamma = 100$ s^{-1} is a numerical constant, and $A_{\alpha,\min}$ is the surface area of a sphere of volume V_α. As far as breakage is concerned, since usually this phenomenon is not very important for particles of small size, only a simple constant kernel was used ($b_{\alpha\beta} = b_0 = 100$ s^{-1}). For the daughter-distribution function symmetric breakage was considered (see Eq. 8). As initial conditions, a monodisperse population of particles with initial number density of $m_{00}(0) = 10^4$ m^{-3} was used. The evolution of the particulate system was calculated for a simulation time that guaranteed significant changes in the distribution, and resulted in a final intensity or extent of aggregation equal to around 0.99, where this quantity is defined as follows

$$I_{agg}(t) = 1 - \frac{m_{00}(t)}{m_{00}(0)}. \tag{29}$$

This final value for the extent of aggregation was chosen because it is often used as benchmark for testing different methods. Of course comparisons could be carried out for longer times since both DQMOM and MCM can handle it, resulting in smaller values of I_{agg}. In Monte Carlo simulations this can be done by doubling the number of particles when a limiting lower value is reached (see Eqs. 25 and 26). However, this comparison leads to very similar results, in fact, after a certain extent, aggregation generates a self-similar normalized distribution, not affecting anymore the quality of the final predictions. For this reason it is also very useful to report the results obtained in dimensionless form. For example, normalizing the moments with respect to their initial values, and making the time dimensionless by normalization with respect to the initial characteristic aggregation time $\tau_c = [4a_0 m_{00}(0)]^{-1}$, it is possible to show that results from test cases with different kinetic parameters in dimensionless form collapse into one single curve. DQMOM simulations result in this case in the solution of a system of ordinary-differential equations, that can be handled with a stiff numerical solver, whereas Monte Carlo simulations were carried out using 10 subvolumes of volume 10^{-1}m^3, each of them containing 10^4 particles, and the probability of escaping from a subvolume to another was set to zero, so that all the particles evolve within the initial reservoir, and the system is homogeneous. The situation corresponds to averaging ten different realizations of the process, each one with 10^4 particles. The restructuring process was simulated outside the Monte Carlo algorithm, by updating the whole particle population (that is, the values of internal coordinates for each particle) at every time-step ($\Delta t = 0.0001s$), according to the restructuring rate.

The other case investigated is the extension of the previous case to an inhomogeneous system with spatial gradients, where particle diffusion only (that is, without particle convection) was considered ($\Gamma = 0.13$ m^2/s) in a one-dimensional (1-D) domain of size $0 < x < L = 1$ m. The kinetic parameters were the same as in the previous case, and two different initial conditions were tested. At first the value of the internal coordinates was held constant throughout the whole domain, while the particle concentration was set to different values in each half of the domain, equal to 1.6×10^5 m^{-3} and to 8×10^4 m^{-3}. Second, the total particle-number density was set equal to 8×10^4 m^{-3} in the whole domain, and two monodisperse population of particles were initialized in the two halves of the domain. In the second half ($x > 0.5L$) the initial volume and surface area were double than in the first half ($x \leq 0.5L$). DQMOM leads in this case to the solution of a set of partial-differential equations that can be easily solved by finite-difference discretization. As far as Monte Carlo simulations are concerned, a 1-D domain is built using the possibility to set different probabilities of escaping from one reservoir to another. For instance, a purely diffusive problem can be set up by fixing equal to 0.5 the probability of moving to reservoir $j + 1$, and that of moving to reservoir $j - 1$, for a particle escaping from reservoir j, while all the other probabilities are set equal to 0. Of course, probabilities of escaping from reservoir 1 to reservoir 2, and from reservoir $N - 1$ to reservoir N are both equal to 1. The frequency of escape from one reservoir to another is determined by the reciprocal of the residence time in each reservoir, which is proportional to the diffusion coefficient.

Eventually a real 2-D system is investigated. DQMOM is implemented in the commercial CFD code Fluent 6.2 to study soot nanoparticles formation and evolution in a turbulent flame. The test case chosen is the ethylene-air turbulent flame (A) studied by Kent and Honnery,[46] for which some experimental data on temperature and soot volume fraction are available. In this flame a round turbulent jet of ethylene is burned in still air at atmospheric pressure; the fuel is injected through a nozzle with diameter equal to 3 mm at 322 K with a jet velocity equal to 52 m/s. In this case, the standard k-ε model can be used as turbulence model whereas the turbulence-chemistry interaction can be described under the hypothesis of instantaneous chemical equilibrium and assuming a β-distribution for the composition probability-density function (PDF). Soot particles are usually in the submicrorange, and they follow the fluid streamlines so that single-phase assumption can be made.

Nucleation and growth rates of soot particles are expressed as a function of acetylene concentration; this key compound along with other 18 radical and molecular species was included in the equilibrium computation. Soot particles undergo Brownian aggregation and therefore the kernel assumes the functional form reported in Eq. 27 where $a_0 = 2k_BT/3\mu$, and where k_B is the Boltzmann constant, T is the absolute temperature, and μ is the fluid viscosity. Often a correction expressed in terms of the Knudsen number (that is, the ratio between the mean-free-path of gas molecules and the particle radius) is applied as explained by Fuchs.[47] Restructuring is described using Eq. 3, and the restructuring rate is assumed to be proportional to the shear rate inside one turbulent eddy $\gamma = \sqrt{\upsilon/15\varepsilon}$, where υ is the kinematic viscosity, and ε is the turbulent-dissipation rate.

Simulations were carried out with a 2-D conformal grid with 10,500 rectangular cells, whereas DQMOM transport equations were implemented in Fluent by using user-defined subroutines. Details concerning the kinetics expressions used to simulate this process can be found in our previous work.[2]

Results and discussion

Let us consider the case of aggregation of solid nanoparticles in which both volume and area are additive in the aggregation event with simultaneous restructuring/sintering. If two nodes ($N = 2$) are used then six moments are needed to generate the linear system. The first five pure moments (that is, m_{00}, m_{10}, m_{01}, m_{20}, m_{02}) are always included, as they represent important physical meanings (particle-number density, mean and variance of internal coordinates), leaving to the sixth moment the only available degree of freedom. As said before, this moment cannot be m_{11}, because this gives rise to a singular matrix. All the other choices of integer mixed moments of global order $(k + l)$ up to five have been investigated.

For order lower than two the choice of the set of moments is not particularly crucial, since most of the tested combinations resulted in very good agreement with Monte Carlo simulations (that is, errors smaller than 5 %), but of course the situation is rather different for higher-order moments.

This can be clearly seen in Figure 2, where the prediction for a moment of global order two is analyzed with the first five moments fixed (m_{00}, m_{10}, m_{01}, m_{20}, m_{02}), and with the sixth moment equal to a moment of global order three, four or five. As it is seen, notwithstanding the choice of the sixth

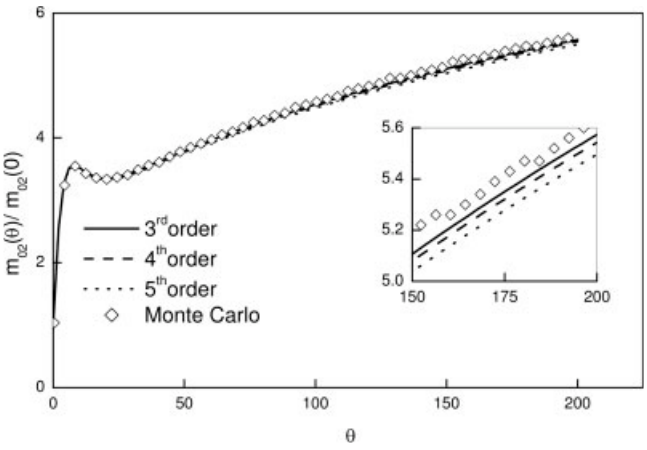

Figure 2. Predictions of m_{02} by DQMOM with $N = 2$ with different choices for the sixth moment, given the first five (m_{00}, m_{10}, m_{01}, m_{20}, m_{02}), vs. dimensionless time σ.

Lines: DQMOM; symbols: Monte Carlo.

moments the agreement with DQMOM and Monte Carlo simulations is always excellent. As it has been anticipated, for higher-order moments the situation is very different, and results for a mixed moment of global order four are shown in Figure 3. It is clear that DQMOM predicts accurately the evolution of the particulate system if the moment (or a moment of the same global order) is included in the set of tracked moments, as it is seen in Figure 3b. If a higher-order moment is instead included (Figure 3c) m_{31} is overpredicted, whereas if a smaller order moment is included m_{31} is underpredicted (see Figure 3a).

In Figure 4 the relative errors affecting the predictions of the integer-mixed moments of order up to five at $I_{agg} = 0.99$ are plotted for some representative choices of the sixth moment. As it has been already reported moments of order up to two are affected by an error smaller than 5%, while moments of higher-global order are affected by higher errors. It is important to highlight here that moments of global order less than or equal to two are the tracked moments, or in other words are directly calculated in DQMOM, whereas higher-order moments are extrapolated. In general, the accuracy of DQMOM with $N = 2$ in tracking low-order moments is acceptable although higher accuracy is possible if three nodes are used. Therefore, if it is necessary to predict with very high-accuracy moments of order higher than two, a formulation with three nodes should be used.

When three nodes are employed for the quadrature approximation, one needs to choose nine mixed moments. Since we are mainly interested in the moments up to order two, tracking all the integer mixed moments of order up to two (that is, the first six integer mixed moments, m_{00}, m_{10}, m_{01}, m_{20}, m_{11}, m_{02}) is a reasonable choice. In this way, one needs to choose three more moments among the ones of order equal to or larger than three.

In Figure 5 the relative errors affecting the predictions of the integer-mixed moments of global order up to five at $I_{agg} = 0.99$ are plotted for a fixed choice of the first six moments (that is, m_{00}, m_{10}, m_{01}, m_{20}, m_{11}, m_{02}), and for four different

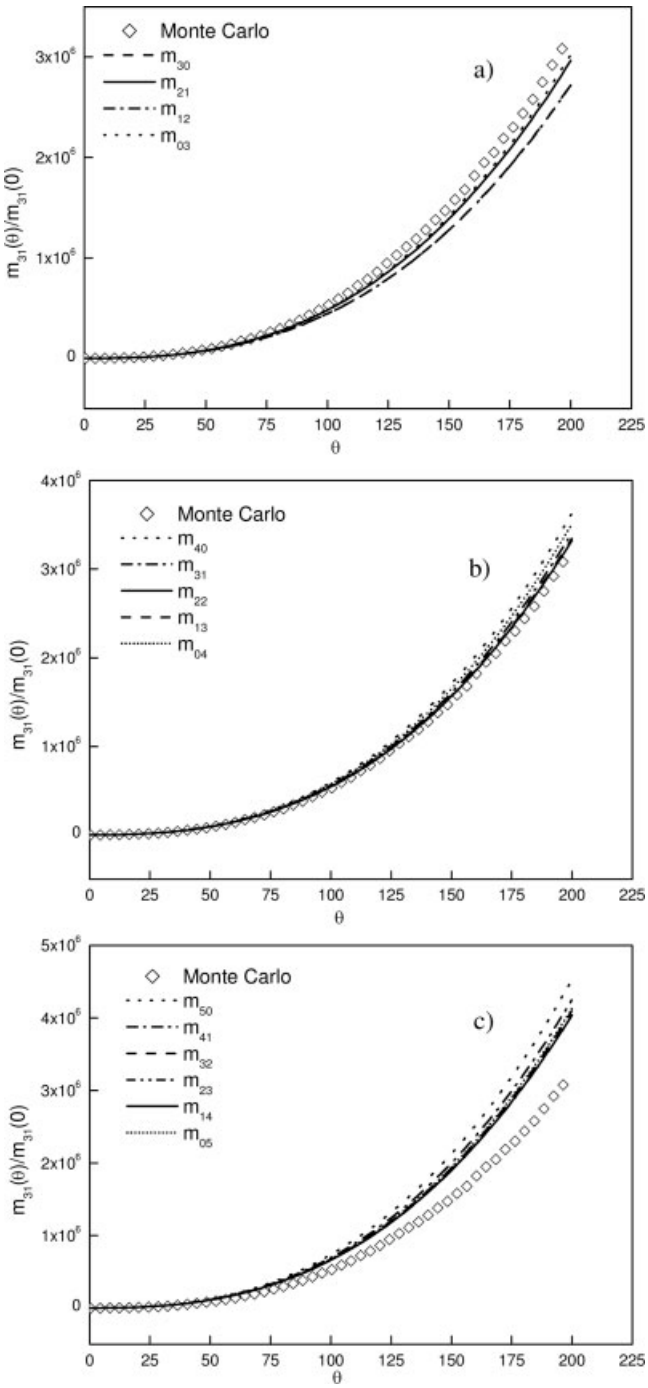

Figure 3. Predictions of m_{31} by DQMOM with $N = 2$ with different choices for the sixth moment among the moments of global order three (a), global order four (b), and global order five (c), given the first five integer pure moments (m_{00}, m_{10}, m_{01}, m_{20}, m_{02}).

Lines: DQMOM; symbols: Monte Carlo.

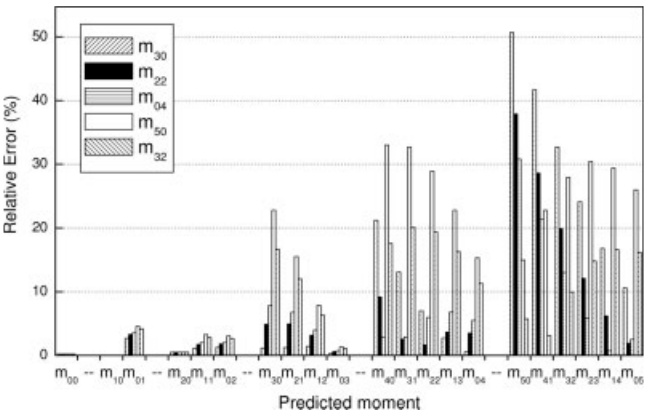

Figure 4. Relative errors for DQMOM with $N = 2$ on the predictions of the integer moments (abscissa) at $I_{agg} = 0.99$ with different choices for the sixth moment (see legend), given the first five (m_{00}, m_{10}, m_{01}, m_{20}, m_{02}).

nodes errors on higher-order moments can still be high, unless a moment of the same order is included in the set of moments used to derive the linear system. It is, therefore, possible to conclude that the number of nodes of the quadrature approximation, and the moments to be included in the set of tracked moments must be carefully chosen. As a general rule, one should always include in the set of tracked moments the higher-order moment that must be accurately predicted.

In order to analyze the importance of the discretization error (that is, the number of nodes) with respect to the round-off error, the results obtained with two or three nodes with double precision were compared to those obtained with single precision. The results have shown that the effect of the discretization error is dominant. For example, using, m_{00}, m_{10}, m_{01}, m_{20}, m_{02}, m_{30} for the simulation with two nodes, and m_{00}, m_{10}, m_{01}, m_{20}, m_{02}, m_{30}, m_{21}, m_{12} for the simulation

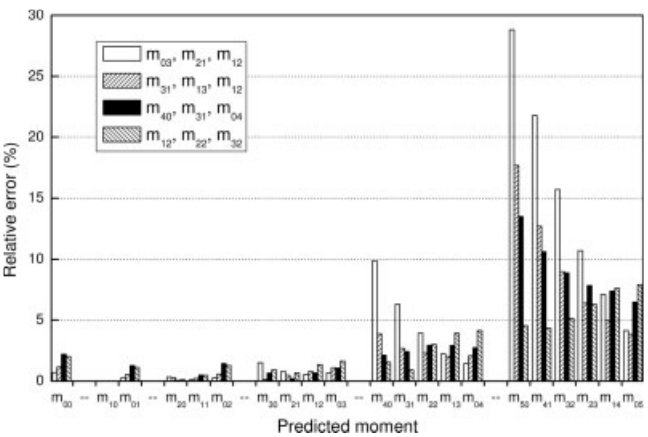

Figure 5. Relative errors for DQMOM with $N = 3$ on the predictions of the integer moments (abscissa) at $I_{agg} = 0.99$ with different choices for the last three moments (see legend), given the first six integer mixed moments (m_{00}, m_{10}, m_{01}, m_{20}, m_{11}, m_{02}).

terns of moments. Comparison of Figures 4 and 5 shows that the use of three nodes leads to a significant improvement, in fact relative errors on predicted moments are reduced by almost one-order of magnitude. However, also with three

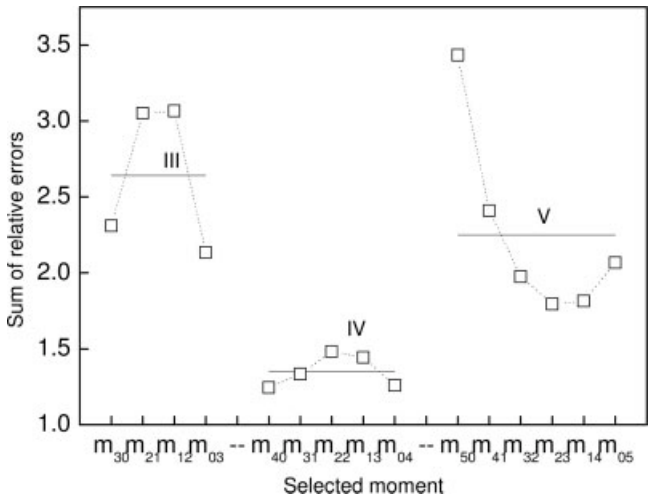

Figure 6. Sum of the relative errors on moments of order up to five, with different choices for the sixth moment, fixed the first five integer pure moments.

The horizontal lines indicate the average value among chosen moments of the same order.

with three nodes, the relative error with respect to the Monte Carlo result at the end of the computation is 0.98% for $N = 3$ with double precision, and is increased to 1.6% for $N = 3$ with single precision, to 8.35% for $N = 2$ with double precision, and to 10.6% for $N = 2$ with single precision.

The analysis of the sum of relative errors for $N = 2$ on moments up to the fifth order, whose behavior is shown in Figure 6 as a function of the selected sixth moment, evidences that the global error is minimized if the set of six moments necessary with two nodes is completed with a moment of order four. Of course, this result is significant only if the goodness of the prediction is evaluated on average on all the mixed integer moments up to the fifth order; it is worth to remind that the choice of the moments to be tracked should always be driven by the selection of the most important moments for the application under investigation. Also in this case, the use of three nodes improves the accuracy of the prediction, and should be considered if the knowledge of higher-order moments is needed, even if, as observed, DQMOM with two nodes performs quite well in this case.

Although for nanoparticles usually breakage is not very important, some comparisons were carried out by using a constant breakage kernel ($b_\alpha = 10^2$ s^{-1}), because in this case the competition between aggregation and breakup results in a steady-state solution, and DQMOM can be tested to correctly predict it. As for the previous case the prediction for low-order moments is excellent. Nevertheless, simulations showed that the steady-state value of higher-order moments is strongly affected by the choice of the sixth moment to be tracked, and that in some cases using two nodes it is not possible to rely on the prediction of the tracked higher-order moments. For the computation of the relative error, the asymptotic value reached by the Monte Carlo simulation was calculated by averaging the values for $800 \leq \theta \leq 2000$. As before, for $N = 2$ the error is acceptable for moments of global order equal or less than two, whereas is generally very large, and not acceptable for moments of order four and five.

Also in this case, a significant improvement can be obtained using the formulation with three nodes. For example, results for a moment of global order equal to three obtained with all the possible terns of moments of order three, four or five, are reported in Figure 7. In the graph, the grey band includes all the curves obtained using a tern of moments of order three, four, or five to complete the set of nine mixed moments. In this case, the prediction of m_{30} is quite good if any tern of moments of order three are used, while using higher-order moments results in an overestimation of the same moment, as expected. However, if moments of higher global order are considered (results not reported here), the predictions are worse, as expected, but the best choice is not anymore the use of terns of moments of the same global order.

Particularly interesting is the extension to a spatial 1-D system. This particular case is very important in order to investigate the role of the correction terms that arise from the finite-mode representation of the distribution and diffusion. The conclusions drawn for this test case can moreover be extended to 2-D and 3-D problems, since the nature of the numerical issue remains the same, changing only the way in which the gradients appearing in the correction term (see Eq. 15) are calculated. In order to assess the ability of the Monte Carlo code and of DQMOM to correctly describe particle diffusion, the two methods were tested in a simple case with diffusion only. The concentration of particles was set constant along all the 1-D domain, and the internal coordinates in one half of the domain were set double than those in the other half. A representation of the domain is depicted in Figure 8. As it is seen in Figure 9, a perfect agreement between Monte Carlo and DQMOM with two nodes (with

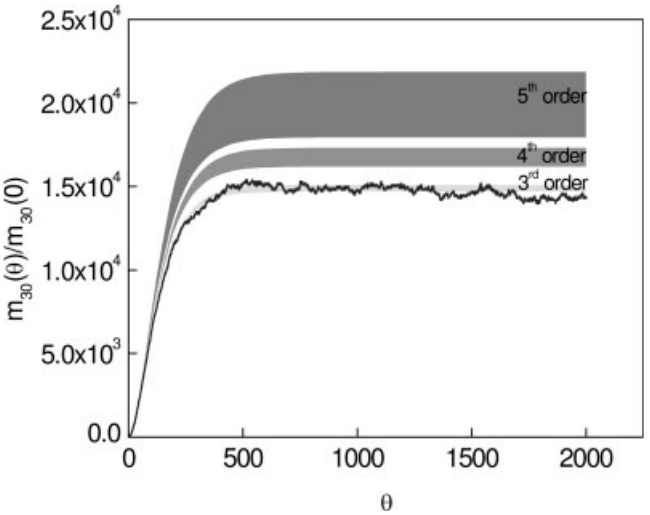

Figure 7. Predictions of m_{30} by DQMOM with $N = 3$, with different choices for the last three moments among moments of global order three, global order four, and global order five, given the first six (m_{00}, m_{10}, m_{01}, m_{20}, m_{11}, m_{02}).

Thin lines: DQMOM; thick line: Monte Carlo.

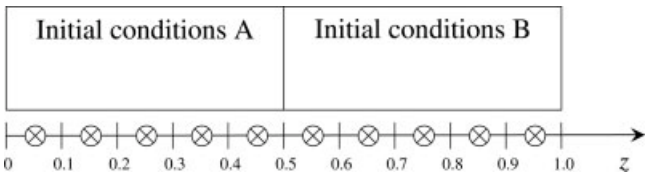

Figure 8. 1-D system employed for simulations with aggregation and diffusion.

The symbols (⊗) identify the subvolumes of the Monte Carlo method.

the following choice of the moments: m_{00}, m_{10}, m_{01}, m_{20}, m_{02}, m_{30}) was found for the prediction of the time evolution of mean-particle volume. The ten lines refer to evenly spaced spatial position along the spatial dimension of the domain (that is, to the ten subvolumes of the Monte Carlo method), therefore, we can conclude that both Monte Carlo simulations and DQMOM accurately describe purely diffusive processes.

For the first initial condition tested (internal coordinates constant throughout the whole domain with gradient in particle concentration) the comparison of relative errors between DQMOM and Monte Carlo simulation in the case of two nodes (m_{00}, m_{10}, m_{01}, m_{20}, m_{02}, m_{30}), and three nodes (m_{00}, m_{10}, m_{01}, m_{20}, $m_{02,}$ m_{21}, m_{12}, m_{30}, m_{03}), for the overall mixed moments up to order five is reported in Figure 10. In this figure predictions for a population of particles undergoing aggregation and diffusion until I_{agg} reaches 0.99 are reported. As expected, the accuracy that can be obtained by using a higher-order quadrature approximation tracking a larger number of moments is usually significantly higher; however, the predictions of DQMOM with three nodes are in some cases worse than the ones obtained with two nodes. Figure 10 confirms as well that the error on the prediction grows as the order of the mixed moment is increased. Errors are acceptable for moments of global order equal to or less than three, whereas generally they are not negligible for moments of global order equal to or higher than four. As usual, the relative error is larger for moments with higher partial order with respect to particle volume, but this is related to the particular case under investigation. The behavior of the DQMOM with two nodes seems to be less regular from this point of view.

In Figure 10, the importance of the correction for the spurious terms is also highlighted by the comparison of relative errors, which are always significantly higher for the simulations in which the correction terms have been neglected. It is worth to note that, even if in this case the population of particles was initially monodisperse, node gradients arise due to the different collision rates in the two compartments of the domain, and to the simultaneous diffusion.

For the second initial conditions (uniform particle concentration throughout computational domain and different initial values of internal coordinates) the time evolution of axial profiles of mean-particle volume (m_{10}/m_{00}), and surface area (m_{01}/m_{00}), as computed by the Monte Carlo algorithm and the DQMOM with three nodes ($N = 3$, moments tracked: m_{00}, m_{10}, m_{01}, m_{20}, $m_{02,}$ m_{21}, m_{12}, m_{30}, m_{03}), is depicted in Figure 11, showing a good agreement between the two methods. These quantities are not affected by the spurious terms, as they depend on moments of global order lower than two.

The axial profiles of two higher-order mixed moments (m_{02} and m_{31}) are reported in Figure 12 for some evenly spaced temporal locations, both with and without the correction for the spurious terms. The figure shows that, when the correction is not applied, the mixed moments are usually underestimated. The importance of the correction is more marked for higher-order moments, but already for moments of order two the effect is significant, especially in the central part of the domain, where the gradients are higher. Therefore, the correction terms should be always taken into account in the simulation when more detailed information on the bivariate number-density function is needed, while they can be neglected with no additional error when the only im-

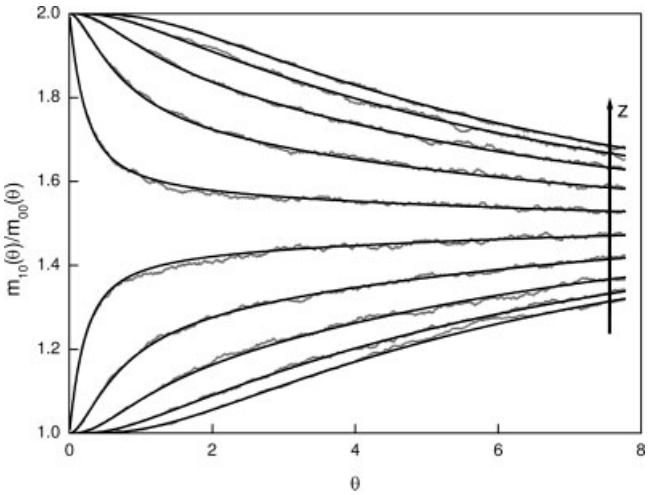

Figure 9. Comparison between Monte Carlo (gray lines) and DQMOM with $N = 2$ (black lines) for the prediction of time evolution of particle volume in the case of diffusion only.

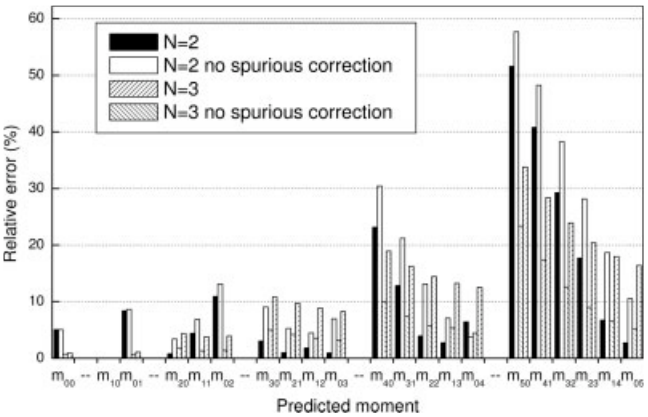

Figure 10. Relative errors on the predictions of the overall integer moments (abscissa) at I_{agg} = 0.99.

Comparison between the formulations of DQMOM with two (m_{00}, m_{10}, m_{01}, m_{20}, m_{02}, m_{30}), and three nodes (m_{00}, m_{10}, m_{01}, m_{20}, $m_{02,}$ m_{21}, m_{12}, m_{30}, m_{03}), with and without the correction for the spurious terms.

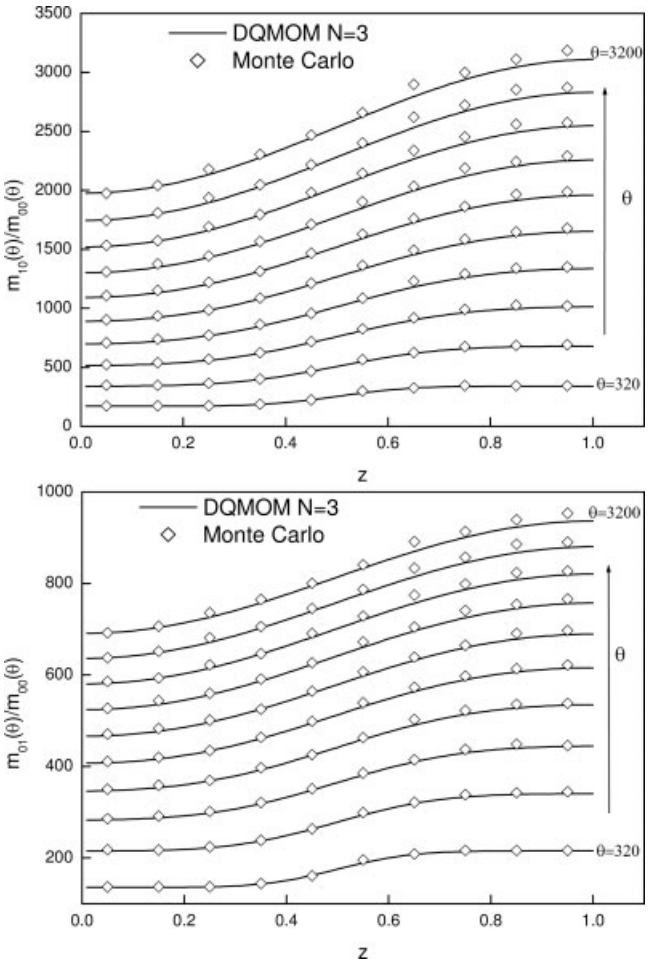

Figure 11. Axial profiles of mean particle volume and surface area.

Comparison between Monte Carlo (symbols), and DQMOM with $N = 3$ (solid lines).

portant information is the evolution of the mean value of the internal coordinates.

Eventually a real 2-D application is investigated: simulation of nucleation, growth, aggregation and restructuring of soot nanoparticles in a turbulent flame. First the mathematical model has been validated through comparison against experimental data found in literature[46] for temperature (not shown here), and soot volume fractions. In Figure 13 radial profiles of soot volume fractions predicted by the bivariate DQMOM implemented in the CFD code at several axial positions are reported. As it is seen agreement is satisfactory, showing that the turbulence model, as well as the turbulence-chemistry interaction approach and the kinetic expressions are describing rather accurately the process. Calculations carried out assuming that soot particles have no effect on the flow field (that is, frozen flow field), and considering the effect of soot particles on the radiative heat transfer (that is, updated flow field), resulted in very similar predictions, showing that the two-way coupling between flame and soot particles is in this case negligible.

In Figure 14 contour plots of flame temperature, mean-particle volume (m_{10}/m_{00}) and mean-particle surface area (m_{01}/m_{00}) are reported. As it is possible to see, as soon as fuel and air mix together combustion takes place resulting in very high-temperature values. This is also the acetylene rich region, where most of the nucleation occurs. Nucleated particles then continuously change their size because of molecular growth, and simultaneously undergo Brownian aggregation and restructuring. The importance of using the bivariate population-balance equation can be inferred by comparing the particle volume and surface area profiles reported in Figure 14. In fact, only a bivariate formulation is capable to predict the independent evolution of these two quantities, as in the last part of the flame, where particle volume still increases, whereas particle surface area decreases.

This application is also very interesting to estimate typical computational times for the simulation of a standard problem. CPU times of the full CFD model on a dual processor Xeon (3.00 GHz) are of about an hour for the flow, turbulence and temperature field and of the same order of magnitude for the solution of the population-balance equation. It is noteworthy to point out here that the addition of the population-balance equation with DQMOM did not change the order of magnitude of the CPU time required, making it possible for the simultaneous solution of the flow field and the population-balance equation (that is, solution of problems with two-way coupling).

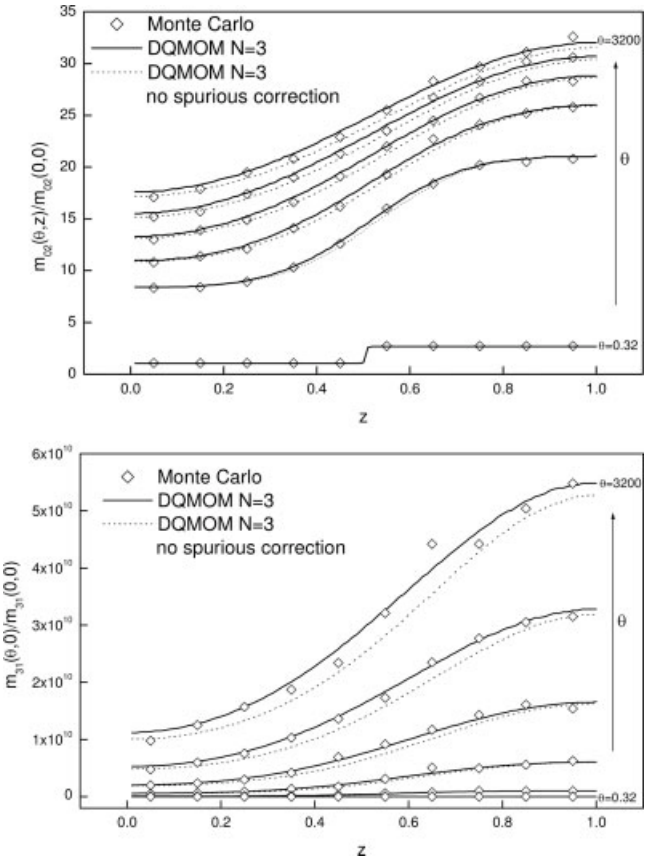

Figure 12. Axial profiles of mixed moments.

Comparison between Monte Carlo (symbols) and DQMOM with $N = 3$ (solid lines) with and without the correction for the spurious terms.

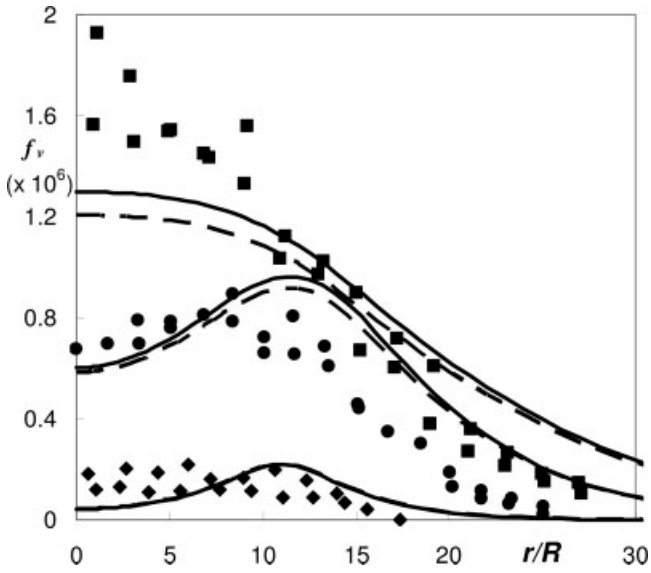

Figure 13. Comparison between experimental data and model predictions of radial profiles of soot volume fraction.

The radial coordinate is normalized with respect to the nozzle radius $R = 1.5$ mm; Experimental data: (◆) axial position x = 138 mm; (●) axial position x = 241.5 mm; (■) axial position x = 345 mm. Continuous line: model predictions with updated flow field. Dashed line: model predictions with frozen flow field neglecting the two-way coupling due to soot radiative heat transfer.

Conclusions

The study of the cases considered in this work provides a validation of DQMOM for simulating formation and evolution of nanoparticles undergoing Brownian aggregation and sintering/restructuring, and it suggests some criteria for the appropriate selection of moments to be tracked to generate the linear system that defines the source terms for the weights and abscissas. In particular, the comparison with results of Monte Carlo simulations has shown that the choice of the tracked moments can affect significantly the accuracy and the numerical stability of the method. The choice of lower-order moments benefits the conditioning of the problem, but it is important to include in the set of the tracked moments those of main interest, or at least moments of the same global order. The use of a higher number of nodes improves the performance of the method, but numerical difficulties can arise as the rank of the linear system is increased. With this respect a solution that deserves to be investigated in our future work is the use of fractional moments, that can help in reducing the condition number of the linear system, thus improving both accuracy and stability. The study of the 1-D diffusion system has evidenced the importance of taking into account the correction for the spurious terms in order to avoid significant errors in the prediction of higher-order moments. Eventually the 2-D application presented clearly showed that DQMOM can be easily implemented in CFD codes, resulting in affordable CPU times for the solution of complex problems.

Acknowledgments

Partial financial support to this research by the Italian Ministry of University and Research (M.I.U.R. - PRIN Project 2003: *Combustion formed particulate: mechanisms of formation, low-emission technologies, health and climate effects*) and by Regione Piemonte (Project: *Study and modeling of fine powders formation processes in combustion*) is gratefully acknowledged.

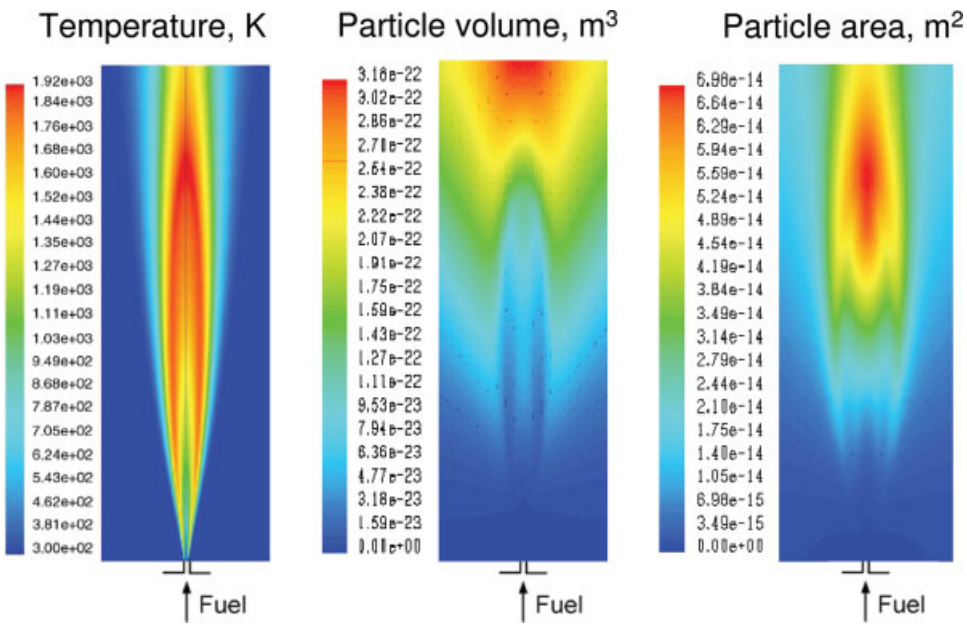

Figure 14. From left to right: temperature, mean particle volume, and mean particle surface area predicted by the bivariate population balance model for the flame under investigation.

[Color figure can be viewed in the online issue, which is available at www.interscience.wiley.com.]

Literature Cited

1. Richter H, Howard JB. Formation of polycyclic aromatic hydrocarbons and their growth to soot-a review of chemical reaction pathways. *Prog Ener Comb Sci*. 2000;26:565–608.
2. Zucca A, Marchisio DL, Barresi AA, Fox RO. Implementation of the population balance equation in CFD codes for modelling soot formation in turbulent flames. *Chem Eng Sci*. 2006;61:87–95.
3. Yu S, Kasibhatla PS, Wright DL, Schwartz SE, McGraw R, Deng A. Moment-based simulation of microphysical properties of sulfate aerosols in the eastern United States: Model description, evaluation, and regional analysis. *J Geophysical Res D: Atmospheres*. 2003;108: AAC4/1–25.
4. McGraw R, Wright DL. Chemically resolved aerosol dynamics for internal mixtures by the quadrature method of moments. *J Aer Sci*. 2003;34:189–209.
5. Rosner DE, Pyykönen JJ. Bivariate moment simulation of coagulation and sintering nanoparticles in flames. *AIChE J*. 2002;48:476–491.
6. Patil KC, Aruna ST, Ekambaram S. Combustion synthesis. *Current Opinion in Solid State & Material Science*. 1997;2:156–l65.
7. Pratsinis SE. Flame aerosol synthesis of ceramic powders. *Prog Energy Comb Sci*. 1998;24:197–219.
8. Pope SB. *Turbulent Flows*. Cambridge University Press: Cambridge; 2003.
9. Hilbert R, Tap F, El-Rabii H, Thévenin D. Impact of detailed chemistry and transport models on turbulent combustion simulations. *Prog Energy Comb Sci*. 2004;30:61–117.
10. Ramkrishna D. *Population Balances: Theory and Applications to Particulate Systems in Engineering*. Academic Press: New York; 2000.
11. Hounslow MJ, Ryall RL, Marshall VR. A discretized population balance for nucleation, growth, and aggregation. *AIChE J*. 1988;34: 1821–1832.
12. Kumar S, Ramkrishna D. On the solution of population balance equations by discretization – I. A fixed pivot technique. *Chem Eng Sci*. 1996;51:1311–1332.
13. Kumar S, Ramkrishna D. On the solution of population balance equations by discretization – II. A moving pivot technique. *Chem Eng Sci*. 1996;51:1333–1342.
14. Hulburt HM, Katz S. Some problems in particle technology. *Chem Eng Sci*. 1964;19:555–574.
15. Diemer RB, Olson JH. A moment methodology for coagulation and breakage problems: Part 2 – Moment models and distribution reconstruction. *Chem. Eng. Sci*. 2002;57:2211–2228.
16. McGraw R. Description of aerosol dynamics by the quadrature method of moments. *Aerosol Sci Tech*. 1997;27:255–265.
17. Marchisio DL, Vigil RD, Fox RO. Quadrature method of moments for aggregation-breakage processes. *J Colloid Inter Sci*. 2003;258: 322–334.
18. Marchisio DL, Pikturna JT, Fox RO, Vigil RD, Barresi AA. Quadrature method of moments for population balances. *AIChE J*. 2003;49: 1266–1276.
19. Barrett JC, Webb NA. A comparison of some approximate methods for solving the aerosol general dynamic equation. *J Aersol Sci*. 1998;29:31–39.
20. Wang L, Marchisio DL, Vigil RD, Fox RO. CFD simulation of aggregation and breakage processes in laminar Taylor-Couette flow. *J Colloid Inter Sci*. 2005;282:380–396.
21. Upadhyay RR, Ezekoye OA. Evaluation of the 1-point quadrature approximation in QMOM for combined aerosol growth laws. *J Aerosol Sci*. 2003;34:1665–1683.
22. Marchisio DL, Vigil RD, Fox RO. Implementation of the quadrature method of moments in CFD codes for aggregation - breakage problems. *Chem Eng Sci*. 2003;58:3337–3351.
23. Pyykönen JJ. Computational simulation of aerosol behaviour. *VTT Publications*. 2002;461:3–70.
24. Wright DL, McGraw R, Benkovitz CM, Schwartz SE. Six-moment representation of multiple aerosol populations in a sub-hemispheric chemical transformation model. *Geophysical Res Letters*. 2000;27:967–970.
25. Wright DL, Kasibhatla PS, McGraw R, Schwartz SE. Description and evaluation of a six-moment aerosol microphysical module for use in atmospheric chemical transport models. *J Geophysical Res D: Atmospheres*. 2001;106:20275–20291.
26. Wright DL, McGraw R, Rosner DE. Bivariate extension of the quadrature method of moments for modeling simultaneous coagulation and sintering of particle populations. *Journal of Colloid and Interface Science*. 2001;236, 242–251.
27. Yoon C, McGraw R. Representation of generally mixed multivariate aerosols by the quadrature method of moments: I. Statistical foundation. *J Aerosol Sci*. 2004;35:561–576.
28. Yoon C, McGraw R. Representation of generally mixed multivariate aerosols by the quadrature method of moments: II. Aerosol dynamics. *J Aerosol Sci*. 2004;35:577–598.
29. Bove S, Tron S, Hjertager BH. A novel algorithm for solving population balance equations: The parallel parent and daughter classes. Derivation, analysis and testing. *Chem Eng Sci*. 2005;60:1449–1464.
30. Fan R, Marchisio DL, Fox RO. Application of the direct quadrature method of moments to polydisperse gas-solid fluidized beds. *Powder Tech*. 2004;139:7–20.
31. Marchisio DL, Fox RO. Solution of population balance equations using the direct quadrature method of moments. *J Aerosol Sci*. 2005; 36:43–73.
32. Park SH, Rogak SN. A one-dimensional model for coagulation, sintering, and surface growth of aerosol agglomerates. *Aerosol Sci Tech*. 2003;37:947–960.
33. Mandelbrot BB. *The Fractal Geometry of Nature*. W. H. Freemand & Company: New York; 1983.
34. Artelt C, Schmid HJ, Peukert W. On the relevance of accounting for the evolution of the fractal dimension in aerosol process simulations. *J Aerosol Sci*. 2003;34:511–534.
35. Filippov AV, Zurita M, Rosner DE. Fractal-like aggregates: relation between morphology and physical properties. *J Colloid Inter Sci*. 2000;229:261–273.
36. Koch W, Friedlander SK. The effect of particle coalescence on the surface area of a coagulating aerosol. *J Colloid Inter Sci*. 1990;140:419–427.
37. Ayazi Shamlou P, Stravrinides S, Titchener-Hooker N, Hoare M. Growth-independent breakage frequency of protein precipitates in turbulently agitated bioreactors. *Chem Eng Sci*. 1994;49:2647–2656.
38. Kramer TA., Clark MM. Incorporation of aggregate break-up in the simulation of orthokinetic coagulation. *J Colloid Inter Sci*. 1998;216: 116–126.
39. Rosner DE., McGraw R, Tandon P. Multivariate population balances via moment and Monte Carlo simulation methods: an important sol reaction engineering bivariate example and mixed moments for the estimation of deposition, scavenging, and optical properties for populations of nonsperical suspended particles. *Ind Eng Chem Res*. 2003;42: 2699–2711.
40. Gordon RG. Error bounds in equilibrium statistical mechanics. *J Math Physics*. 1968;9:655–667.
41. Ducoste J. A two-scale PBM for modeling turbulent flocculation in water treatment processes. *Chem Eng Sci*. 2002;57:2157–2168.
42. Liffman K. A direct simulation Monte-Carlo mehtod for cluster coagulation. *J Comp Physics*. 1992;100:116–127.
43. Garcia ALC, Van den Broek C, Aertsens M, Serneels R. A Monte Carlo method for coagulation, *Physica*. 1987;143A:535–548.
44. Gillespie DT. Exact method for numerically simulating the stochastic coalescence process in a cloud. *J Atmospheric Sci*. 1975:32: 1977–1989.
45. Kruis FE, Maisels A, Fissan H. Direct simulation Monte Carlo method for particle coagulation and aggregation. *AIChE J*. 2000;46: 1735–1742.
46. Kent JH, Honnery D. Soot and mixture fraction in turbulent diffusion flames. *Comb Sci Tech*. 1987;54:383–397.
47. Fuchs NA. *Mechanics of Aerosols*. Pergamon Press: New York, 1964.

Manuscript received Feb. 3, 2006, and revision received Nov. 22, 2006.